Engineering Structures 306 (2024) 117810

Contents lists available at ScienceDirect

Engineering Structures

journal homepage: www.elsevier.com/locate/engstruct

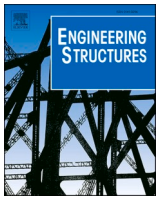

Parametric fire curves for I-girder bridges submitted to under deck tanker fires

Jethro David Howard [a], Ignacio Paya-Zaforteza [b,*], Guillem Peris-Sayol [c]

[a] Universitat Politècnica de València, Spain
[b] ICITECH, Universitat Politècnica de València, Spain
[c] Departamento de Ingeniería Mecánica, Universidad Pontificia Comillas, Spain

ARTICLE INFO

Keywords:
Bridge fire
Fire curve
Bridge resilience
Computational Fluid Dynamics
Performance-based design

ABSTRACT

Bridge fires are of significant concern due to their potential consequences and the absence of standards for assessing fire resistance in bridges. The first step in this assessment involves building a fire model, often using Computational Fluid Dynamics (CFD) models. While CFD models are accurate, they are complex to build.

This paper introduces closed-form expressions for parametric fire curves for I-girder bridges exposed to fires provoked by a burning tanker under the bridge mid-span or close to its abutments/piers. These fire curves eliminate the need for building CFD models and depend on key parameters defining the bridge (substructure configuration, width, span, vertical clearance) and the fire load (Heat Release Rate). The fire curves provide the adiabatic surface temperatures heating the bridge deck and their variation along the bridge deck longitudinal axis. The fire curves were obtained through a multi-step process that involved: a) a comprehensive design of experiments to define combinations of parameters used to build representative CFD models of I-girder bridges under fire, b) the use of ANOVA models to identify the most relevant parameters and parameter interactions, c) the use of multiple linear regression to derive the mathematical expressions, i.e. the fire curves, fitting the results of the CFD models run in the design of experiments step, d) a validation of the proposed fire curves for combinations of parameters not considered in the design of experiments. The resulting parametric fire curves are straightforward linear equations and can be easily generated with a spreadsheet provided as a Supplementary material. Consequently, these parametric fire curves represent a practical tool for both academics and practitioners interested in evaluating the fire resistance of I-girder bridges. This marks a significant step forward in enhancing bridge resilience against fire hazards.

1. Introduction

Given the importance of bridges in infrastructure networks, the scientific-technical community has devoted a great effort to protecting them against extreme load events, such as earthquakes, winds, scour, and ship collisions (see e.g Ghosn et al. [1]). Several studies [2–5] have shown that fire is another major hazard for bridges and have stressed the failure of current codes to guide on how to protect bridges from fire. This lack of standards contrasts with the potential grave consequences of bridge fires as illustrated by the fire under the MacArthur Maze in Oakland, USA on April 29th 2007. This fire was provoked by the overturning of a tanker truck and caused the collapse of two spans of the Maze 22 min after the beginning of the fire. Repairs and rebuilding operations costed more than US $9 million and indirect costs due to traffic detours were estimated to be US $6 million per day [3]. Another more recent example of the consequences of bridge fires is a vehicle fire under the I-95 highway near the Cottman Avenue exit in Northeast Philadelphia, on June 11, 2023, which caused a portion of the highway to collapse, resulting in the closure of a segment that carried around 160,000 vehicles per day, of which roughly 14,000 were trucks [6].

Despite the important consequences of bridge fires, fire engineering has traditionally focused on mitigating the effects of fires on buildings and tunnels (see e.g. [7–12]). However, bridge fires are very different from tunnel and building fires [13,14] and require a specific approach. This need has motivated a lot of research (see [3,4,15,16] for detailed literature reviews) that mainly focused on: (a) risk analyses and probabilistic studies (e.g. [17]), (b) numerical studies on the fire response of bridges (e.g. [13,18–27]) (c) experiments carried out in open air

* Corresponding author.
E-mail addresses: jetho@upv.es (J.D. Howard), igpaza@cst.upv.es (I. Paya-Zaforteza), gperis@icai.comillas.edu (G. Peris-Sayol).

https://doi.org/10.1016/j.engstruct.2024.117810
Received 9 November 2023; Received in revised form 10 February 2024; Accepted 3 March 2024
Available online 19 March 2024

conditions (e.g. [14,28]) or in a lab furnace (e.g. [29–31]), and (d) systems to protect bridges from fire (e.g. [32]). Among all these studies, works with numerical models are the most common since they predict the fire response of a bridge and define protective measures when required, and are also helpful to analyze the structural condition of a bridge after a fire.

Numerical studies of bridges under fire require three types of models: (a) a fire model which indicates how the bridge is heated, (b) a thermal model to obtain the temperatures within the bridge structure depending on its heating, and (c) a structural model to obtain the bridge mechanical response. Fire models are, thus, the first step in any numerical analysis of a bridge fire and have different levels of complexity. The simplest fire models are the nominal temperature-time curves such as the ISO 834 (typically used in buildings), the RWS (typically used in road tunnels) or the hydrocarbon fire curves. More realistic and complex are the natural fire models that consider the characteristics of both the fire source and the fire compartment. EN 1991–1-2 [33] describes natural fire models which, among others, include: parametric curves for buildings (Annex A), a localized fire model valid for fires with heat release rates (HRR) smaller than 50 MW (Annex C) and the more advanced zone models and Computational Fluid Dynamics models (Annex D). Bridge fires happen in open air conditions, with no oxygen limitation, and have fast heating rates and high intensities. These conditions make fire curves developed for buildings and tunnels not suitable. In addition, and according to the statistical study by Peris-Sayol et al. [2], the worst scenarios in terms of bridge damage, are those where a tanker starts a fire under a bridge and these fires have HRR higher than 50 MW. As a result, the localized fire model of EN 1991–1-2 and the fire models developed for tunnels and buildings cannot be applied. Different approaches have tried to overcome this difficulty. Pioneering works (Choi [34], Alos-Moya et al. [18]), used Computational Fluid Dynamics (CFD) to model the fire source and the bridge with its environment to obtain the spatial and temporal distribution of the variables describing the heating of bridge decks. CFD can provide accurate results, but they are complex to build and require important calculation times, which has motivated the development of alternative procedures. Ma et al. [35] proposed a semi-empirical fire model to obtain flame temperatures corresponding to fires provoked by different types of vehicles located on the bridge deck, therefore, with no restriction to the extension of the flames in the vertical direction. This study also considered the influence of wind. Wu et al. [36] modified the localized fire model presented in the SFPE Handbook [37] for its application to fire scenarios where a tanker truck is burning under box girder bridges. The model was then applied to evaluate the fire response of a post-tensioned segmental concrete box girder bridge submitted to a fire under the bridge mid-span cross-section. The model by Wu et al. [36] assumes that, at each heated bridge cross-section, fire exposure is uniform, i.e., all the exposed faces of the webs and flanges of the box girder are heated with same temperature.

Within this context, this study proposes closed form expressions for parametric fire curves specific for I-girder bridges submitted to under deck tanker fires, the tanker being placed at two potential positions: under the bridge mid-span and close to its piers or abutments. In addition to the tanker position, the expressions also consider the most relevant factors affecting fire development: vertical clearance, bridge span, bridge width, structural configuration, and heat release rate of the fire (related to type of fuel). Therefore, the study is very relevant because:

- I-girder bridges and similar structures constitute a very important part of bridge inventories. For example, and according to data compiled in [38], these systems counted for 47,65% of all bridges and represented 69,55% of all bridge deck surfaces included in the US National Bridge Inventory.
- I-girder bridges are especially vulnerable to under-deck tanker fires. The statistical analysis of 154 bridge fires by Peris-Sayol at al. [2] showed that 77% of the bridges that collapsed or suffered a massive damage that provoked their demolition used this structural system.
- Parametric fire curves for I-girder bridges submitted to under deck fires do not exist. Previous works are very relevant but focus on fires caused by vehicles on the deck [35] or on box girders where each deck cross section is uniformly heated [36]. However, fire exposure is not uniform in I-girder bridges submitted to under deck fires. Hot gases concentrate in the volume between two adjacent I-girders and, as a result, fire exposure in the bottom flange of the girder is significantly different to fire exposure on its web and top flange (see e.g. Peris-Sayol et al. [39]). In addition, the model proposed by Wu et al. [36] considers the longitudinal evolution of the temperatures along the bridge, but it does not take into account the position of the fire source with respect to the bridge piers or abutments. This position is very relevant because, due to the Coandă effect [40], fire exposure on the bridge deck when the tanker is close to the bridge abutments is different to fire exposure when the fire source is under mid-span and, typically, the former exposes the deck to much higher temperatures (see [39]).
- The fire curves proposed are expressed in terms of adiabatic surface temperatures and, therefore valid for steel, concrete and composite bridges.

The paper is structured as follows: Section 2 describes the general pattern of the proposed fire curves, which are defined in terms of adiabatic surface temperatures and consist of a growing phase followed by a steady burning phase characterized by a steady burning adiabatic temperature. Section 3 outlines the methodology used to derive closed-form expressions for these steady burning adiabatic temperatures based on the study's considered parameters. In addition, Section 3 presents these closed-form expressions, which undergo discussion and validation in Section 4 through CFD simulations. Lastly, Section 5 summarizes the main conclusions of this work.

2. General pattern of the parametric curves

Fire curves are mathematical expressions which represent the temporal evolution of the thermal actions impinging a structure during a fire and combine, in a single temperature, the effects of convection and radiation. In general, the progression of a fully developed fire goes through three phases: growth, steady burning and decay (Fig. 1a). Correspondingly, fire curves describing realistic fire scenarios have a pattern that replicates these stages with some variations as seen in Fig. 1b.

When defining a fire curve corresponding to a tanker burning under the bridge deck, it should be considered that:

- Bridge fires occur in the open air with no oxygen limitation and, therefore, they are fuel-controlled.
- Peris-Sayol et al. [2] showed that incidents involving tanker trucks carrying gasoline produced a higher average damage to bridges than tankers carrying other types of fuel. This happened because gasoline has a higher heat release rate than other fuels [42] and is highly flammable at ambient temperatures. Therefore, the proposed fire curves should be consistent with the features of hydrocarbon fires, which have a very high heating rate, i.e., reach very high temperatures in short periods of time.
- During the fire, temperatures experiment significant variation along the bridge axis as shown by previous experimental and numerical studies [14,18,39]. Therefore, it is not possible to heat the full bridge girders length with a single fire curve.

  Within this context, the parametric fire curves proposed assume that every bridge girder receives the same heat flux which is applied as follows (see Fig. 2 and Fig. 3):
- The bridge girder is divided in longitudinal segments (Fig. 2a). At each heated section, and following previous results [18], two different heating patterns are introduced: a first one to heat the top slab, top flange and web, and a second one to heat the bottom flange (Fig. 2b).

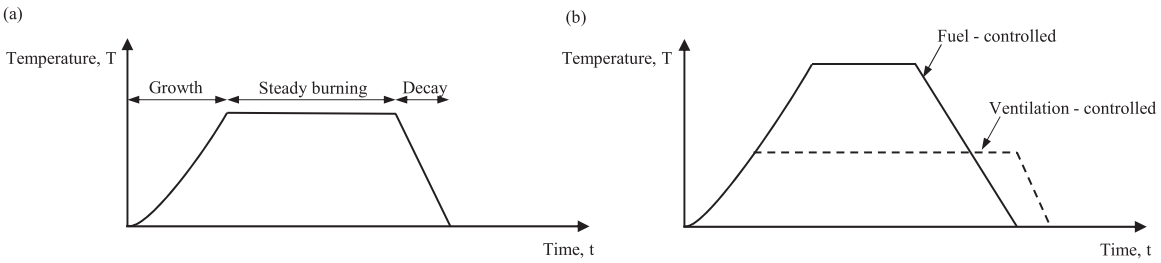

Fig. 1. (a) Typical phases of a fire. (b) Comparison between a fuel-controlled fire and a ventilation-controlled fire. Adapted from Mayfield and Hopkin [41].

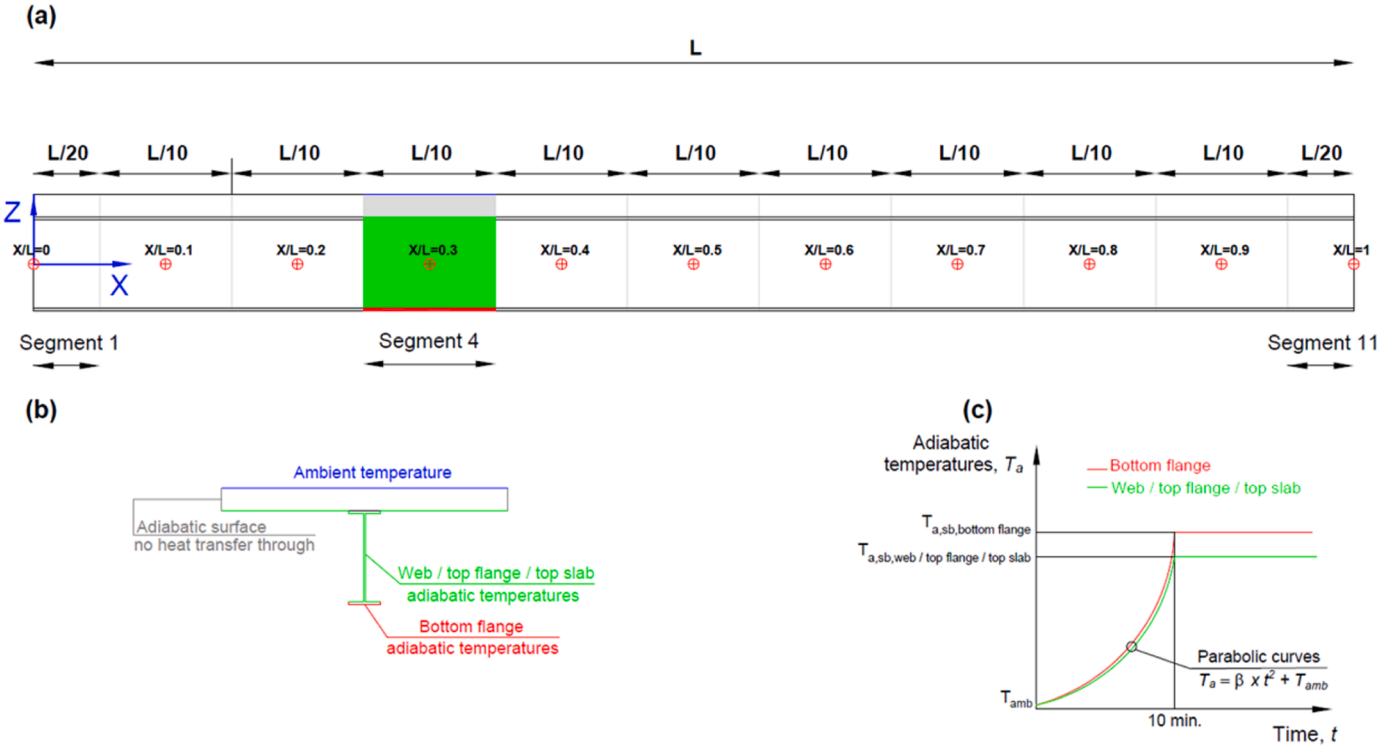

Fig. 2. (a) Division of a typical girder in segments. Different colors in Segment 4 represent different thermal boundary conditions. (b) Thermal boundary conditions applied in each girder segment. (c) Generic form of the proposed parametric fire curves.

- The fire curves are defined in terms of adiabatic surface temperatures T_a or, briefly, adiabatic temperatures. This concept was developed by Wickström et al. [43] and corresponds to a fictitious temperature obtained assuming that the structural element is a perfect insulator. Its use for bridge fires was validated in previous works [18,27,44] and enables: 1) to transform the radiation and convection heat fluxes impinging the bridge surface into an equivalent gas temperature adjacent to that surface, and 2) the introduction of the fire model results in the thermo-mechanical model. In addition, adiabatic temperatures are independent of the structural material of the bridge girders and, thus, can be applied to steel, concrete and steel-concrete composite bridges. The emissivity factors of the materials that form the I-girder and/or bridge deck are introduced in the thermal model to carry out the heat transfer analysis using the previously obtained adiabatic surface temperatures T_a.
- The proposed fire curves have the two phases shown in Fig. 2c: growth and steady burning adiabatic temperature ($T_{a,sb}$ henceforth). It must be noted that:

1. It is not necessary to define a decay stage because typically, firefighters arrive at the fire scene or the bridge collapses before temperatures start to decrease due to fuel consumption. For example, if the fire load is a tanker truck carrying 35 m^3 of gasoline with a density of 740 kg/m^3 and an effective heat of combustion of 43.7 MJ/kg [45], then the energy released during the fire is 970140 MJ. If the fire corresponds to a confined pool fire (i.e. without oil spill) then a heat release rate per unit area (HRRPUA) of 2.4 MW/m^2 can be assumed [39,45]. If the tanker surface is 30 m^2 (see e.g. [46]), then the total HRR would be 72 MW and, using the methodology presented in [45], the duration of the fire in the absence of extinguishing measures would be four hours and 21 min. This time is much longer than the time it took bridges to collapse because of a fire (e.g. the first span of the MacArtur Maze collapsed 17 min after the beginning of the fire, and the second span collapsed after 20 min [47]) and it exceeds the time firefighters would typically need to reach the bridge fire location.
2. The growth phase is modeled assuming the fire is an ultrafast t-squared fire where the relation between *HRR* (in MW) and time t (in seconds) since the beginning of the fire is given by Eq. 1 (see [42]).

$$HRR(t) = 1.874 \times 10^{-4} \times t^2 \quad (1)$$

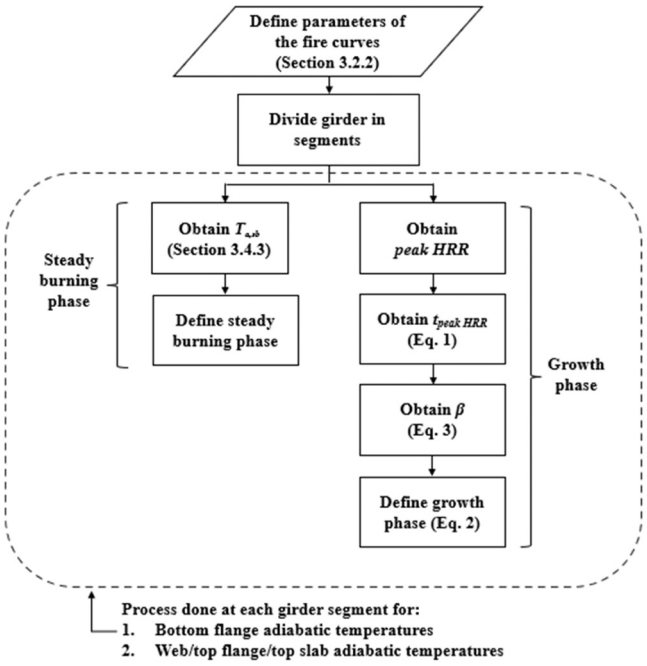

Fig. 3. Flowchart summarizing the process of definition of the parametric fire curves.

However, parametric fire curves do not depict HRR temperature relationships, but rather time-temperature relationships with a growth phase expressed by Eq. 2:

$$T_a(t) = \beta \times t^2 + T_{amb} \tag{2}$$

where β is a coefficient and T_{amb} is a constant equal to the ambient temperature (typically 20 °C). Additional calculations are required to obtain β. Firstly, the time required to reach the *peak HRR* ($t_{peak\ HRR}$) is derived by solving t for the *peak HRR*. For instance, for a *peak HRR* of 72 MW corresponding to a 30 m^2 tanker fire, the peak is reached after 620 s of fire duration (or roughly 10 min). Then, β can be calculated using Eq. 3, derived from Eq. 2 considering that $T_a(t_{peak\ HRR}) = T_{a,sb}$.

$$\beta = \frac{T_{a,sb} - T_{amb}}{t_{peak\ HRR}^2} \tag{3}$$

3. $T_{a,sb}$ is obtained using the procedure detailed in Section 3.4.3.

3. Calculation of steady burning adiabatic temperatures

3.1. Introduction

The key element to define the parametric fire curves is the steady burning adiabatic temperature $T_{a,sb}$. This temperature is provided in the form of closed-form expressions obtained through to the following process:

1) A design of experiments (DOE henceforth) is first carried out to define both, the parameters (e.g. span length or vertical clearance) to be considered, and the number of bridge configurations needed to guarantee the statistical significance of the results obtained. See details in Section 3.2.
2) Steady burning adiabatic temperatures $T_{a,sb}$ in the I-girder surfaces are obtained for each significant configuration. These temperatures are obtained with Computational Fluid Dynamic models of each configuration run with the software Fire Dynamics Simulator (FDS) [48], which has been validated for similar problems by contrast with observations from real bridge fire events [18,27] and with experiments with a real bridge built at the campus of the Universitat Politécnica de Valencia [14,44]. See details in Section 3.3. $T_{a,sb}$ values are analyzed using the analysis of variance (ANOVA) technique to obtain the significance of each parameter considered. The parameters (and interactions) having a significant effect on the steady burning adiabatic temperatures are used to build a predictive model using multiple linear regression. The combination of predictive models for various points along the bridges span provides the heating curves. See details in Section 3.4.
3) Finally, to validate the predictive model, heating curves provided by the predictive model are compared with heating curves obtained with FDS, for the following three groups: parameter values used to obtain the predictive models, parameter values that fall within the studied ranges (interpolation), and parameters that fall outside these ranges (extrapolation). See details in Section 4.

3.2. Design of experiments

3.2.1. Parameters selection

This study considers a total of five parameters to characterize $T_{a,sb}$. Four of them relate to the bridge geometry (structural configuration, width, span and vertical clearance), whilst the fifth parameter is the HRRPUA and characterizes the design fire. The analysis also considers two potential positions of the burning tanker: under the bridge mid-span or adjacent to the pier/abutment.

Whist the number of potential fire source shapes and positions is infinite, this paper has chosen to consider a large tanker truck [46] located under the central I-girder and perpendicular to the deck, based on numerous previous events of similar characteristics and their potential to cause the most severe damage to bridge structures [2]. Considering two tanker truck positions (close to the abutments / piers and under mid-span) is the logical choice because:

- In simply supported decks, these tanker positions provoke the maximum heating of the sections close to the abutments or piers (where shear forces are the highest) and of the mid-span sections (where positive bending moments are the highest).
- In continuous decks, these tanker positions provoke the maximum heating of the sections close to the abutments or piers (where shear forces and negative bending moments are the highest) and of the mid-span sections (where resistance vis-à-vis positive bending moments is crucial).

To reduce the total number of simulated configurations, other parameters which are not expected to have influence such as the production of smoke (soot) and the production of carbon monoxide (CO yield) are not considered. According to existing publications on standard bridge designs [49], the distance between the axis of two adjacent I-girders is taken as 2.6 m and the girders depth as 0.8 m. Preliminary calculations showed that transverse girders (diaphragms) do not have any significant influence on the steady burning adiabatic temperatures [50], and thus have not been included in the FDS models.

3.2.2. Parameters definition

Each of the selected parameters is defined as follows (see Fig. 4):

- Substructure configuration defines the type of deck support for the span where the fire source is located, with it being considered identical at either end.
- Width is defined as the total width of the deck top slab, measured from between each exterior face.
- Span is the distance between the faces of abutments or the faces of piers for each respective bridge substructure configuration.

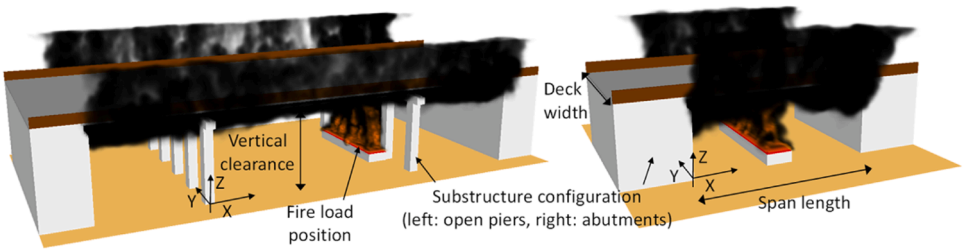

Fig. 4. Graphical definition of the parameters.

- Vertical clearance is the distance between the road surface/pavement and the lower face of the bottom flange of the I-girders.
- HRRPUA is the heat release rate per unit area, applied to a horizontal surface of 28.8 m^2 (12 m x 2.4 m) located 1 m above road surface/pavement.

The values chosen for each parameter (see Table 1) are based on the following:

- Substructure configuration: the two types proposed are commonly used in I-girder bridges.
- Width: the proposed range covers the most common values of deck width for single and dual carriageway roads or highways, including additional space for shoulders, pavements, and road barriers.
- Span: the proposed range covers the most common values of span length for I-girder bridges, crossing either single or dual carriageway roads and/or highways.
- Vertical clearance: the lower limit aligns with the typical minimum vertical clearance mandated by highway design standards. It is worth noting that overpasses often maintain a vertical clearance close to this minimum requirement to minimize the height of approaching embankments and consequently reduce costs. The upper limit is chosen based on previous results by Peris-Sayol et al. [39].
- HRRPUA: the value of 2400 kW/m^2 is based on the HRRPUA of gasoline according to SFPE [46]. For the lower value of the HRRPUA, 1800 kW/m^2 has been chosen because according to the formulation of SFPE [46], the HRRPUA for diesel can range from 1800 to 1950 depending on the pool depth and diameter, and the composition of diesel.

3.2.3. Number of configurations

A standard 2^k factorial design [51] has been used for the DOE, where k represents the number of parameters considered (thus $k = 5$). The number of FDS models required per position is $2^5 = 32$, and as two burning tanker positions are considered, a total of 64 models are needed. Note that sometimes fractional factorial designs using e.g. the Taguchi method [52] are used to reduce the number of configurations needed to cover all possible parameter combinations. However, this reduction has not been applied here to obtain complete information on the main effects (individual effects of each factor) and interactions (combined effects of factors). By doing so a precise estimation of all main effects and interactions can be achieved.

Table 1
Definition of parameter levels.

Substructure configuration	Width (m)	Span (m)	Vertical Clearance (m)	HRRPUA (kW/m^2)
Deck supported on open piers (e.g. monolithic frames or hammer head piers)	13	16	5	2400
Deck supported on abutments or solid wall piers	23.4	24	9	1800

3.3. FDS analysis

3.3.1. Introduction

A Fire Dynamics Simulator (FDS) model for each of the sixty-four configurations presented in Table 2 was setup, requiring the definition of control volumes (including boundary conditions and mesh discretization), the geometrical definition of the bridge, its material properties (including both adiabatic and non-adiabatic surfaces), the fire source, a combustion model, sensors to record the models output, etc. Details of these FDS models are given in Table 3.

3.3.2. Boundary conditions

As seen in Table 3 there are two main types of boundary conditions in the FDS models: the adiabatic surfaces, such as the bridges superstructure (I-girders and deck), and the nonadiabatic surfaces, as in the case of the abutments and/or piers. In the case of the nonadiabatic surfaces, the materials are defined within the FDS model, and therefore these surfaces "absorb" part of the heat emitted by the fire source. The reason for including these nonadiabatic surfaces in the analysis is so that the adiabatic temperatures obtained in the model for the bridge girders/beams consider the influence of the bridge substructures (abutments and/or piers), as these are not included in the thermomechanical analysis.

3.3.3. Sensor location

The number and position of sensors used to record adiabatic temperatures from the computational fluid dynamic models follows the approach proposed by Alos-Moya et al. [18] who concluded that three sensors are sufficient in a typical I-girder bridge cross-section to register the temperatures from the FDS models: one located in the center of the lower face of the bottom flange and the other two positioned in the center of either side of the web. Adiabatic temperatures in the top flange and in the deck slab can be assumed to be the same as those in the corresponding web [18].

3.3.4. FDS Results

All FDS models were run using version 6.6.0, as an MPI parallel job on the Universitat Politècnica de València (UPV) calculation cluster, Rigel. Each model had between three and fifteen cores assigned for the calculations, with 8 GB of RAM per core. Total calculation times for each model varied between eight and thirty-two hours. Each model provided between 243243 and 363363 temperature readings (depending on the span of each model, either 16 or 24 m.), as values were recorded approximately every 0.15 s, for a total of 150 s, for each of the sensors located along the central I-girder, for both the bottom flange and either side of the web.

The adiabatic temperatures registered for each sensor throughout the FDS analyses need postprocessing which implies: (1) removing the fire growth phase, which has been considered to last no longer than 30 s for all models, and (2) obtaining the average adiabatic temperatures during the rest of the analysis, for each of the individual sensors (in the case of the web, the average is obtained considering the sensors on both web faces, as there is no significant difference between adiabatic temperatures measured on each side of the web due to the fire source being

Table 2
Design of Experiments: bridge configurations studied.

Model[a]	Substructure configuration	Width (m)	Span (m)	Vertical clearance (m)	HRRPUA (kW/m^2)
1 / 33	Open piers	13.0	16	5	2400
2 / 34	Open piers	13.0	16	5	1800
3 / 35	Open piers	13.0	16	9	2400
4 / 36	Open piers	13.0	16	9	1800
5 / 37	Open piers	13.0	24	5	2400
6 / 38	Open piers	13.0	24	5	1800
7 / 39	Open piers	13.0	24	9	2400
8 / 40	Open piers	13.0	24	9	1800
9 / 41	Open piers	23.4	16	5	2400
10 / 42	Open piers	23.4	16	5	1800
11 / 43	Open piers	23.4	16	9	2400
12 / 44	Open piers	23.4	16	9	1800
13 / 45	Open piers	23.4	24	5	2400
14 / 46	Open piers	23.4	24	5	1800
15 / 47	Open piers	23.4	24	9	2400
16 / 48	Open piers	23.4	24	9	1800
17 / 49	Abutments or solid wall piers	13.0	16	5	2400
18 / 50	Abutments or solid wall piers	13.0	16	5	1800
19 / 51	Abutments or solid wall piers	13.0	16	9	2400
20 / 52	Abutments or solid wall piers	13.0	16	9	1800
21 / 53	Abutments or solid wall piers	13.0	24	5	2400
22 / 54	Abutments or solid wall piers	13.0	24	5	1800
23 / 55	Abutments or solid wall piers	13.0	24	9	2400
24 / 56	Abutments or solid wall piers	13.0	24	9	1800
25 / 57	Abutments or solid wall piers	23.4	16	5	2400
26 / 58	Abutments or solid wall piers	23.4	16	5	1800
27 / 59	Abutments or solid wall piers	23.4	16	9	2400
28 / 60	Abutments or solid wall piers	23.4	16	9	1800
29 / 61	Abutments or solid wall piers	23.4	24	5	2400
30 / 62	Abutments or solid wall piers	23.4	24	5	1800
31 / 63	Abutments or solid wall piers	23.4	24	9	2400
32 / 64	Abutments or solid wall piers	23.4	24	9	1800

[a] Each line of the table represents two models: one corresponds to the burning tanker located under mid-span (cases 1 to 32), and the other corresponds to the burning tanker located adjacent to piers/abutment (cases 33 to 64)

located right below the central I-girder). Fig. 5 shows a typical output of a sensor from an FDS analysis and Fig. 6 shows how this output is transformed into a discretized curve showing the values of $T_{a,sb}$ along the bridge. Note that:

1) After 150 s, average temperatures remain stable and, therefore, it is not necessary to continue the FDS analysis.
2) $T_{a,sb}$ temperature curves are obtained for both the bottom flange and web of each of the sixty-four FDS models and are discretized into eleven points: X/L= 0, X/L= 0.1, …, X/L= 1 where X is the longitudinal coordinate of the I-girder and L its span (see Fig. 6). In the case of the thirty-two configurations from the scenario where the fire is located under the bridge mid-span, the average temperature for equidistant points on either side of the center (X/L=0.5) is used, reducing the total number of points to be analyzed to six (X/L=0 to X/L=0.5) to obtain symmetric design fire curves, as the differences between each pair of equidistant points is minimal.

Table 3
Details of FDS models.

Control volume	X ∈[34,58] m; Y ∈[30,46] m; Z ∈[12,18] m
Cell size	0.20 × 0.20 × 0.20 m (Fine mesh according to[53])
Fire scenario	Fire area: horizontal surface of 28.8 m^2 (12 m x 2.4 m) located 1 m above road level. CO yield = 0.019; Soot yield = 0.059 according to[54] for hydrocarbon fires
Boundary conditions	Adiabatic surfaces: bridges superstructure (I-girders and deck) Nonadiabatic surfaces: substructures (piers and/or abutments)
Sensors	Three located every 0.2 m along central I-girder: center of the bottom flange and at the center of either side of the web

As an example of the results obtained, Fig. 7 shows two selected FDS curves with the aim of comparing, for a particular case, the influence of having a vertical clearance of 5 or 9 m as well as the influence of the position of the burning tanker. Results show that, when the tanker is under mid-span, the vertical clearance has a major influence and there is a maximum difference in the $T_{a,sb}$ values of 320ºC for the bottom flange and 464ºC for the web. However, when the tanker is adjacent to an abutment or a solid wall pier, vertical clearance does not have a major influence. The latter is the result of the Coandă effect [40] noticed in a previous study by Peris-Sayol [39], in which the flames and/or hot gasses tend to stay attached to the flat surface of the abutment and help them reach larger heights.

In Howard [50], additional graphical comparisons and discussion are provided for other FDS models for the other four parameters (substructure configuration, width, span and HRRPUA).

3.4. Statistical analysis

3.4.1. Introduction

The steady burning adiabatic temperatures for each point of discretization of the FDS curves were analyzed using ANOVA tests [51] to determine the significance of each of the five parameters considered (bridge substructure configuration, width, span, vertical clearance and HRRPUA), as well as their second order interactions. Individual analyses were carried out for both positions of the burning tanker (adjacent to abutment/piers or under mid-span), and for both the bottom flange and web / top flange / top slab. Therefore, a total of thirty-four ANOVA tests were performed, as shown in Table 4 (in the case of the burning tanker located under mid-span, the average temperature for equidistant points on either side of the center is used, reducing the total number of points to be analyzed to six, as explained in Section 3.3.4).

For each of these ANOVA tests, the parameters and interactions which were found to be statistically significant ($p < 0.05$) were used in multiple linear regression (MLR henceforth) models. These MLR models form the basis of the fire design curves, as each model provides a prediction of the steady burning adiabatic temperature for a single point, for fires located under mid-span or adjacent to abutment/piers, and for either the bottom flange or web / top flange / top slab. The combination of all points for each subset provides a set of predictions of the steady burning adiabatic temperatures $T_{a,sb}$ which enables to build the design fire curves along the whole I-girder.

All the analyses used the software Statgraphics [55], which is capable of carrying multifactorial ANOVA tests, and iterative multiple linear regression calculations.

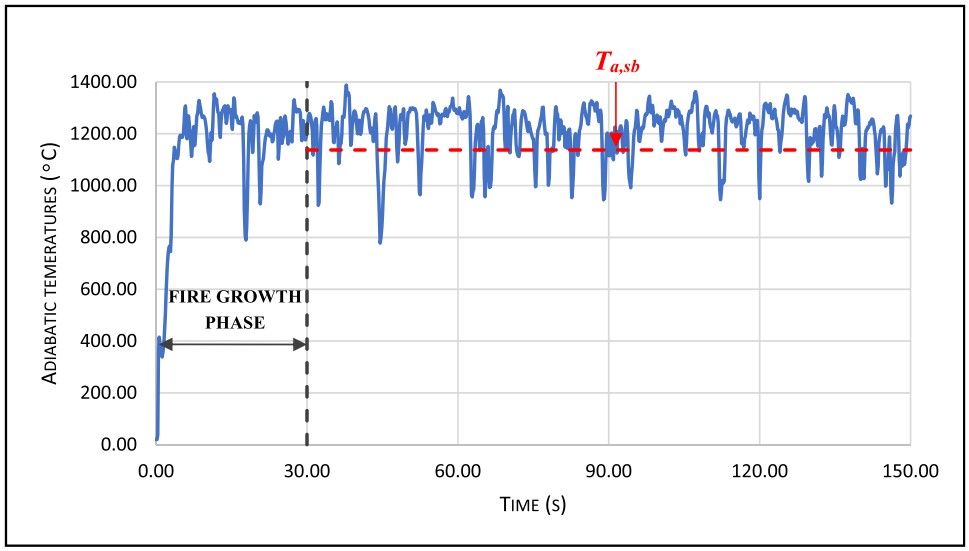

Fig. 5. Example of adiabatic temperatures registered during the FDS analysis of model 13 at X/L= 0.5 for the bottom flange sensor. Note that in this FDS model the growing phase of the fire was not simulated to save computing time.

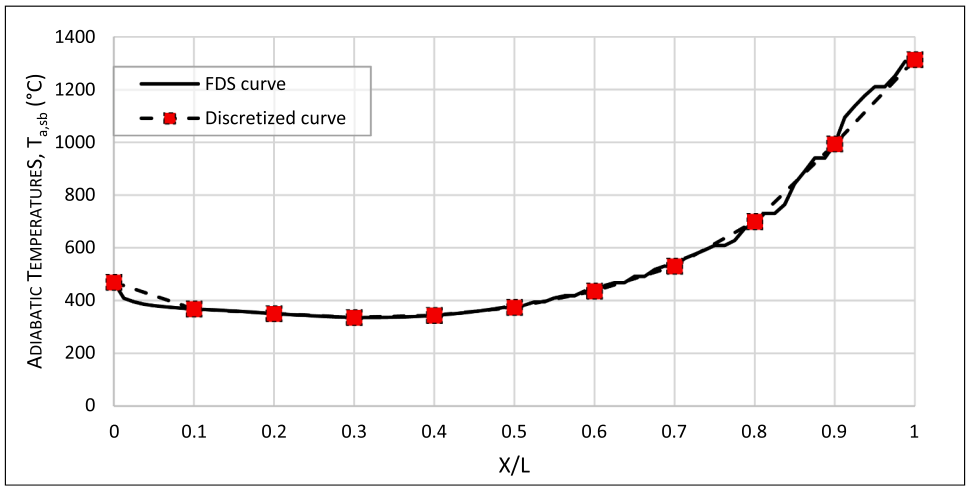

Fig. 6. Example of discretization of steady burning adiabatic temperatures $T_{a,sb}$ along the longitudinal axis of the girder for the bottom flange sensor registered during the FDS analysis of model 33.

3.4.2. *ANOVA results*

The following sections provide a summary of the ANOVA test results related to the steady burning adiabatic temperatures observed for each of the sixty-four bridge configurations analyzed, depending on their relative position.

3.4.2.1. Tanker burning under mid-span. Table 5 and Table 6 present a comprehensive summary of the ANOVA results for the steady burning adiabatic temperatures at various positions along the bridge girder when the tanker burns under mid-span. Results indicate that the majority of parameters significantly influence $T_{a,sb}$, except bridge width, span, and substructure configuration for certain positions. Importantly, when studying the parameters in isolation, some may not exhibit a significant impact, but their influence becomes apparent when considered in combination with other factors, demonstrating second-order effects. For instance, bridge width alone may not significantly impact the steady burning adiabatic temperatures of the bottom flange at position X/L= 0.4 (p-value of 0.0623 in Table 5), yet it is significant at the same location when interacting with the bridge span (interaction bridge width – bridge span with a p-value of 0.0023 in Table 5). These findings underscore the importance of studying parameter combinations to fully understand their influence on $T_{a,sb}$.

3.4.2.2. Tanker burning adjacent to piers or abutment. A summary of the ANOVA results for the values of $T_{a,sb}$ at different relative positions along the bridge girder for configurations with the fire located adjacent to an abutment or piers are shown in Table 7 for the bottom flange and in Table 8 for the web and top slab.

In the case of the bottom flange steady burning adiabatic temperatures, all five parameters have a significant effect on the values of $T_{a,sb}$ for the majority of the relative positions. In the case of the bridge's width, the ANOVA tests for relative positions near the fire source (X/L = 0.8 to X/L = 1) indicate that this parameter is not statistically significant, as is also the case for the effect of the bridge span in the immediate vicinity of the fire (X/L = 1). It is logical that these parameters have greater significance the further from the fire source, as the temperatures of these relative positions depend more on the absolute distance to the fire, as well as the ventilation conditions.

For the web/top flange/slab values of $T_{a,sb}$, bridge width has a significant effect for all relative positions. This happens because the gasses/

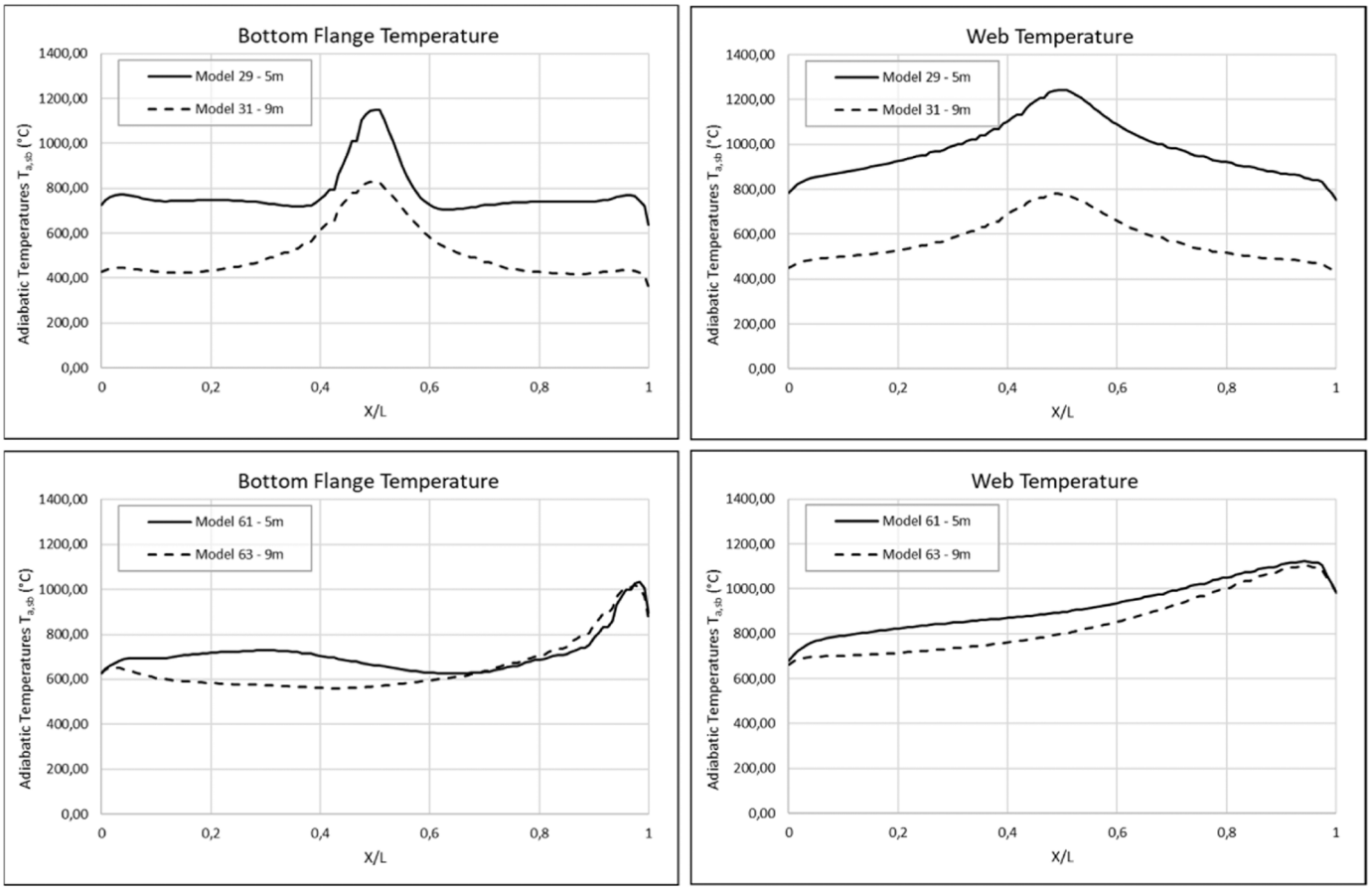

Fig. 7. Comparison of steady burning adiabatic temperatures $T_{a,sb}$ obtained with FDS along the longitudinal axis of the bridge for the models 29 and 31 with burning tanker under mid-span (top) and for the models 61 and 63 with the burning tanker close to the abutment (bottom). In every case, the substructure configuration is "Deck supported on abutment or solid wall piers", HRRPUA is 2400 kW/m^2, bridge span is 24 m and bridge width is 23.4 m.

Table 4
Summary of ANOVA tests performed.

Location of steady burning adiabatic temperatures	Burning tanker position	Number of ANOVA carried out
Bottom flange	Under mid-span	6
Web	Under mid-span	6
Bottom flange	Adjacent to abutment/piers	11
Web	Adjacent to abutment/piers	11

smoke in contact with the web are confined in between neighboring I-girders, and therefore, the greater the width, the more I-girders present, and the more difficult it is for the gasses/smoke in contact with the central I-girder to escape, causing an increased build-up in steady burning adiabatic temperatures.

3.4.3. MLR results

The fitted MLR models obtained for each relative position, for both the bottom flange and web, and depending on the fire location scenario, were used to determine parametric fire curves capable of predicting the steady burning adiabatic temperatures affecting a bridge's superstructure.

As can be seen in Table 9, the adjusted R^2 of all the fitted MLR models is above 0.888, with those considering the burning tanker under mid-span performing better than the those with it adjacent to an abutment or piers.

Results of the proposed parametric fire curves are provided in matrix form in Table 10 to Table 13, which allows the partial regression coefficients and model constant to be viewed for each relative position.

The matrix form of the parametric fire curves can be used to calculate the steady burning adiabatic temperature of the desired relative position

Table 5
Summary of ANOVA test results (p-values) for the bottom flange steady burning adiabatic temperatures when the burning tanker is under mid-span. Values in bold correspond to p-values lower than 0.05, indicating the parameter or the interaction has a statistically significant influence on $T_{a,sb}$.

	X/ L= 0	**X/ L= 0.1**	**X/ L= 0.2**	**X/ L= 0.3**	**X/ L= 0.4**	**X/ L= 0.5**
Main Effects						
A	**0.0000**	**0.0000**	**0.0000**	**0.0000**	**0.0046**	**0.0000**
B	0.0517	**0.0001**	**0.0000**	**0.0030**	0.0623	**0.0014**
C	**0.0000**	**0.0000**	**0.0000**	**0.0000**	**0.0000**	**0.0181**
D	**0.0000**	**0.0000**	**0.0000**	**0.0000**	**0.0000**	**0.0000**
E	**0.0000**	**0.0000**	**0.0000**	**0.0000**	**0.0000**	**0.0000**
Interactions						
AB	0.0051	0.7678	0.7216	0.0731	0.7459	0.0750
AC	**0.0030**	0.8716	**0.0126**	0.5288	0.9762	**0.0023**
AD	**0.0003**	**0.0000**	**0.0000**	**0.0000**	**0.0002**	0.7941
AE	0.4270	**0.0215**	**0.0018**	**0.0032**	**0.0114**	0.0589
BC	**0.0009**	0.1445	0.1557	0.1065	**0.0023**	**0.0311**
BD	0.4185	0.1103	**0.0059**	**0.0028**	0.0629	0.0549
BE	0.7521	0.7568	0.5593	0.7878	0.8683	0.7744
CD	**0.0143**	**0.0012**	**0.0067**	**0.0009**	**0.0000**	**0.0127**
CE	0.3895	0.5471	0.9241	0.1637	**0.0001**	0.3611
DE	0.0731	**0.0006**	**0.0003**	0.1088	**0.0001**	**0.0000**

A: Substructure configuration, B: Width, C: Span, D: Vertical clearance, E: HRRPUA

Table 6
Summary of ANOVA test results (p-values) for the web / top flange / top slab steady burning adiabatic temperatures when the burning tanker is under mid-span. Values in bold correspond to p-values lower than 0.05, indicating the parameter or the interaction has a statistically significant influence on $T_{a,sb}$.

	X/ L= 0	X/ L= 0.1	X/ L= 0.2	X/ L= 0.3	X/ L= 0.4	X/ L= 0.5
Main Effects						
A	**0.0026**	**0.0000**	**0.0000**	**0.0001**	0.8154	**0.0132**
B	0.0976	**0.0349**	0.3709	0.1011	**0.0006**	**0.0006**
C	**0.0000**	**0.0000**	**0.0000**	**0.0000**	**0.0000**	0.4251
D	**0.0000**	**0.0000**	**0.0000**	**0.0000**	**0.0000**	**0.0000**
E	**0.0000**	**0.0000**	**0.0000**	**0.0000**	**0.0000**	**0.0000**
Interactions						
AB	0.2585	0.0898	0.1115	0.5633	0.2573	0.1066
AC	**0.0421**	0.3080	0.2207	0.2376	0.0994	0.0641
AD	**0.0000**	**0.0000**	**0.0000**	**0.0002**	0.1259	0.7239
AE	0.8111	0.1166	0.1116	0.1391	0.1230	0.0969
BC	0.0935	0.1550	0.1043	**0.0391**	**0.0194**	**0.0358**
BD	0.2157	0.5941	0.7941	0.7694	0.2253	0.0934
BE	0.9152	0.8894	0.7888	0.7387	0.8395	0.9846
CD	**0.0000**	**0.0000**	**0.0001**	**0.0009**	0.2715	**0.0111**
CE	0.1080	0.1165	0.1301	0.2007	0.6093	0.6086
DE	**0.0026**	**0.0012**	**0.0034**	0.2300	**0.0045**	**0.0000**

A: Substructure configuration, B: Width, C: Span, D: Vertical clearance, E: HRRPUA

by summing the individual products between the values that appear for the applicable column by the corresponding values of the parameter of that same row. In the case of the constant, it is multiplied by 1, whereas for the interactions of two parameters, both corresponding values for each should be included in the multiplication. Null values in the matrix indicate that those parameters and/or interactions are not significant, either based on the ANOVA tests or as a result of the fitted MLR models.

The following equation (Eq. 4) shows an example of the calculation, using the above fire curves, of the bottom flange steady burning adiabatic temperature, for fires located under the bridge mid-span (Table 10), for relative position X/L= 0:

$$\begin{aligned} T_{a,sb} = {} & 1549.4 - 28.892 \times Width - 54.853 \times Span - 86.848 \\ & \times Vert.Clear. + 0.1836 \times HRR + 6.694 \times Sub.Config. \\ & \times Width + 9.058 \times Sub.Config. \times Span - 29.053 \times Sub.Config. \\ & \times Vert.Clear. + 1.1579 \times Width \times Span + 2.0293 \times Span \\ & \times Vert.Clear. \end{aligned} \quad (4)$$

Note that in Eq. 4, bridge width, span and vertical clearance is introduced in m, HRRPUA is introduced in kW/m^2 and the variable "substructure configuration", which is considered as a dummy variable, equals to 0 when the deck is supported on open piers and 1 when the bridge is supported on solid wall piers or abutments.

A spreadsheet of the parametric fire curve equations from Table 10 to Table 13 is included as supplementary material, providing the predicted steady burning adiabatic temperatures for both bottom flange and the web / top flange / top slab, for both fire locations, in both numerical and graphical formats.

4. Validation

4.1. Introduction

To validate the proposed parametric fire curves, a comparison has been carried out between the steady burning adiabatic temperatures obtained using the proposed parametric fire curves and those obtained from FDS models for equivalent parameter values.

Firstly, some comparisons will be provided from the initial 64 models (training data) used to obtain the parametric fire curves. Following this, additional comparisons will be made with new configurations, both for parameter values that fall within the studied ranges (interpolation) and parameter values that fall outside these ranges (extrapolation), to validate the proposed parametric fire curves.

To evaluate the differences between the steady burning adiabatic temperatures obtained from the FDS analyses and those predicted by the parametric fire curves both a graphical and numerical comparison will be presented. For the former, the corresponding steady burning adiabatic temperatures will be plotted on a graph, whilst for the latter two values will be given: the mean absolute percentage error (MAPE) between each set of steady burning adiabatic temperatures (see Eq. 5), and the percentage error (PE) between the maximum steady burning adiabatic temperatures (see Eq. 6). They are defined as follows:

$$MAPE(\%) = \frac{100}{n} \sum_{i=1}^{n} \left| \frac{T_{a,sb,FC,i} - T_{a,sb,FDS,i}}{T_{a,sb,FDS,i}} \right| \quad (5)$$

Where $T_{a,sb,FC,i}$ is the steady burning adiabatic temperature predicted by the parametric fire curves at a particular point i; $T_{a,sb,FDS,i}$ is the steady burning adiabatic temperature obtained from the FDS analyses at a particular point i; and n is the number points studied. Note that n is equal to 11 for all comparisons, even those where the fire is located mid-span, and the number of points proposed by the fire curve is 6 (since, in this case, the same temperatures are predicted for equidistant points on either side of the center).

Table 7
Summary of ANOVA test results (p-values) for the bottom flange steady burning adiabatic temperatures when the burning tanker is adjacent to piers or abutment (position X/L=1). Values in bold correspond to p-values lower than 0.05, indicating the parameter or the interaction has a statistically significant influence on $T_{a,sb}$.

	X/L= 0	X/L= 0.1	X/L= 0.2	X/L= 0.3	X/L= 0.4	X/L= 0.5	X/L= 0.6	X/L= 0.7	X/L= 0.8	X/L= 0.9	X/L= 1
Main Effects											
A	**0.0000**	**0.0000**	**0.0000**	**0.0000**	**0.0000**	**0.0000**	**0.0000**	**0.0000**	**0.0000**	**0.0066**	**0.0022**
B	0.0963	**0.0033**	**0.0029**	**0.0010**	**0.0002**	**0.0001**	**0.0006**	**0.0252**	0.2391	0.2649	0.5159
C	**0.0001**	**0.0001**	**0.0000**	**0.0000**	**0.0000**	**0.0000**	**0.0000**	**0.0000**	**0.0000**	**0.0000**	0.1824
D	**0.0000**	**0.0000**	**0.0000**	**0.0000**	**0.0000**	**0.0000**	**0.0000**	**0.0000**	**0.0000**	**0.0000**	**0.0000**
E	**0.0100**	**0.0021**	**0.0006**	**0.0002**	**0.0000**	**0.0000**	**0.0000**	**0.0000**	**0.0000**	**0.0000**	**0.0001**
Interactions											
AB	**0.0152**	0.1826	0.2090	0.0754	**0.0092**	**0.0014**	**0.0026**	**0.0436**	0.2438	0.1736	**0.0005**
AC	0.7204	0.2160	0.2312	0.1288	**0.0351**	**0.0166**	0.1346	0.6695	0.1365	0.2746	0.1933
AD	0.0914	**0.0017**	**0.0002**	**0.0000**	**0.0000**	**0.0000**	**0.0000**	**0.0015**	0.5949	**0.0040**	**0.0027**
AE	0.7176	0.3700	0.1489	0.0787	**0.0374**	**0.0186**	**0.0162**	**0.0448**	0.4543	0.4003	0.2520
BC	0.2725	0.9519	0.9690	0.9431	0.7734	0.4614	0.3586	0.4438	0.7951	0.9948	0.1054
BD	**0.0107**	**0.0199**	**0.0267**	**0.0381**	**0.0463**	**0.0353**	**0.0191**	**0.0045**	**0.0019**	**0.0013**	**0.0007**
BE	0.3839	0.3252	0.3491	0.3286	0.3437	0.3204	0.3281	0.4063	0.5632	0.7252	0.7351
CD	0.3479	0.5364	0.4472	0.4782	0.2911	0.1121	0.0949	0.0868	0.3321	0.1991	0.6522
CE	0.9906	0.9441	0.9572	0.9436	0.7513	0.6984	0.8576	0.9116	0.7291	0.7629	0.9747
DE	0.6213	0.8683	0.7259	0.4889	0.3081	0.2189	0.1912	0.2766	0.8268	0.9735	0.3790

A: Substructure configuration, B: Width, C: Span, D: Vertical clearance, E: HRRPUA

Table 8
Summary of ANOVA test results (p-values) for the web / top flange / top slab steady burning adiabatic temperatures when the burning tanker is adjacent to piers or abutment (position X/L=1). Values in bold correspond to p-values lower than 0.05, indicating the parameter or the interaction has a statistically significant influence on $T_{a,sb}$.

	X/L= 0	X/L= 0.1	X/L= 0.2	X/L= 0.3	X/L= 0.4	X/L= 0.5	X/L= 0.6	X/L= 0.7	X/L= 0.8	X/L= 0.9	X/L= 1
Main Effects											
A	**0.0000**	**0.0000**	**0.0000**	**0.0000**	**0.0000**	**0.0000**	**0.0000**	**0.0000**	**0.0000**	**0.0000**	**0.0037**
B	**0.0123**	**0.0080**	**0.0082**	**0.0088**	**0.0116**	**0.0185**	**0.0300**	**0.0376**	**0.0401**	**0.0207**	**0.0306**
C	**0.0001**	**0.0001**	**0.0000**	**0.0000**	**0.0000**	**0.0001**	**0.0002**	**0.0012**	**0.0006**	**0.0158**	0.5011
D	**0.0000**	**0.0000**	**0.0000**	**0.0000**	**0.0000**	**0.0000**	**0.0000**	**0.0000**	**0.0000**	**0.0000**	**0.0000**
E	**0.0018**	**0.0004**	**0.0001**	**0.0001**	**0.0000**	**0.0000**	**0.0000**	**0.0000**	**0.0000**	**0.0000**	**0.0000**
Interactions											
AB	0.1383	0.1196	0.1041	0.0784	0.0607	0.0582	0.0645	0.0644	**0.0495**	**0.0114**	**0.0028**
AC	0.2835	0.2778	0.2702	0.2712	0.2922	0.4012	0.6705	0.9183	0.3100	0.1739	0.6353
AD	0.2632	**0.0229**	**0.0145**	**0.0185**	**0.0382**	0.1168	0.3877	0.8843	0.1021	**0.0002**	**0.0000**
AE	0.9862	0.6907	0.5550	0.5420	0.6339	0.8387	0.8545	0.4931	0.1637	**0.0135**	**0.0171**
BC	0.9234	0.9803	0.9674	0.9431	0.8690	0.7820	0.7828	0.8717	0.9922	0.7894	0.4472
BD	**0.0115**	**0.0098**	**0.0085**	**0.0070**	0.0051	**0.0036**	**0.0026**	**0.0020**	**0.0017**	**0.0008**	**0.0009**
BE	0.3211	0.3392	0.3567	0.3604	0.3681	0.3893	0.4166	0.4644	0.5219	0.5345	0.5009
CD	0.3051	0.3295	0.2821	0.2405	0.2157	0.2664	0.4213	0.5865	0.7272	0.8530	0.8410
CE	0.9315	0.9991	0.9867	0.9453	0.8934	0.9009	0.9422	0.9721	0.8597	0.6673	0.7400
DE	0.8452	0.8399	0.6292	0.4982	0.4297	0.4210	0.4509	0.5187	0.6689	0.8700	0.1756

A: Substructure configuration, B: Width, C: Span, D: Vertical clearance, E: HRRPUA

Table 9
Results of adjusted R^2 of all the fitted MLR models.

	Mean	Interval
Bottom flange temperatures for fire under mid-span	0.977	0.960 – 0.991
Web/top flange/slab temperatures for fire under mid-span	0.995	0.992 – 0.996
Bottom flange temperatures for fire adjacent to an abutment or piers	0.924	0.888 – 0.947
Web/top flange/slab temperatures for fire adjacent to an abutment or piers	0.943	0.900 – 0.956

Table 10
Parametric fire curves coefficients for bottom flange steady burning adiabatic temperatures, for fires located under the bridge mid-span.

	X/L= 0	X/ L= 0.1	X/ L= 0.2	X/ L= 0.3	X/ L= 0.4	X/ L= 0.5
K	1549.400	259.575	353.633	604.840	897.633	1604.010
A	0	294.166	201.616	161.614	0	-157.685
B	-28.892	3.043	7.761	7.460	0	-10.172
C	-54.853	-19.692	-20.725	-19.173	-9.218	0
D	-86.848	0	0	-29.416	-91.303	-133.763
E	0.1836	0.3612	0.2538	0.1333	0.2134	0
AB	6.694	0	0	0	0	0
AC	9.058	0	3.470	0	0	6.001
AD	-29.053	-40.658	-42.747	-30.418	-7.656	0
AE	0	0.0520	0.0615	0.0564	0.0305	0
BC	1.1579	0	0	0	0	0.3865
BD	0	0	-0.6825	-0.8306	0	0
BE	0	0	0	0	0	0
CD	2.0293	1.1648	1.0915	1.2406	1.4116	-1.1260
CE	0	0	0	0	-0.0066	0
DE	0	-0.0284	-0.0163	0	0.0140	0.0322

K: Constant, A: Substructure configuration, B: Width, C: Span, D: Vertical clearance, E: HRRPUA

$$PE(\%) = 100 \times \frac{T_{a,sb,FC,\max} - T_{a,sb,FDS,\max}}{T_{a,sb,FDS,\max}} \quad (6)$$

Where $T_{a,sb,FC,max}$ is the maximum steady burning adiabatic temperature predicted by the parametric fire curves and $T_{a,sb,FDS,max}$ is the maximum steady burning adiabatic temperature obtained from the FDS analyses.

MAPE is preferred over PE to make a global evaluation of each curve defined by a set of steady burning adiabatic temperatures because it does not fall foul of positive and negative forecast errors offsetting each other.

Table 11
Parametric fire curves coefficients for the web / top flange / top slab steady burning adiabatic temperatures, for fires located under the bridge mid-span.

	X/L= 0	X/ L= 0.1	X/ L= 0.2	X/ L= 0.3	X/ L= 0.4	X/ L= 0.5
K	889.731	864.723	908.826	1098.980	1394.490	1813.020
A	121.519	150.983	151.872	93.513	0	-16.494
B	0	0	0	0	-7.689	-10.037
C	-24.747	-22.824	-20.534	-17.476	-12.631	0
D	-81.017	-80.314	-85.001	-111.179	-131.921	-189.030
E	0.3172	0.3407	0.3377	0.2779	0.2125	0
AB	0	1.7709	0	0	0	0
AC	0	0	0	0	0	
AD	-14.896	-18.575	-15.976	-10.193	0	0
AE	0	0	0	0	0	0
BC	0	0	0	0	0.2897	0.3814
BD	0	0	0	0	0	0
BE	0	0	0	0	0	0
CD	1.9265	1.6985	1.3843	1.0677	0	-0.9169
CE	0	0	0	0	0	0
DE	-0.0143	-0.0146	-0.0118	0	0.0127	0.0416

K: Constant, A: Substructure configuration, B: Width, C: Span, D: Vertical clearance, E: HRRPUA

However, in the case of comparing individual points, such as the maximum steady burning adiabatic temperatures of each curve, PE is preferred because it provides a positive or negative result indicating if the predicted values are under or overestimating the actual value.

4.2. Existing models (training data)

As can be seen in Table 14, the results of MAPE values for the existing models are correlated with the coefficient of determination (R^2) values given previously, with steady burning adiabatic temperatures for the burning tanker under mid-span performing better than those with it adjacent to an abutment or piers.

Table 15 provides the results of PE values for the maximum girder steady burning adiabatic temperatures for the existing models. Note that for models with the burning tanker located under mid-span, the maximum girder steady burning adiabatic temperature is always located in position X/L= 0.5. For the models with the burning tanker located adjacent to an abutment or piers, the maximum girder steady burning adiabatic temperature is located in position X/L= 1 with the exception of two cases where the steady burning adiabatic temperatures for the web/top flange/slab are higher for position X/L= 0.9, but the difference

Table 12
Parametric fire curves coefficients for bottom flange steady burning adiabatic temperatures, for fires located adjacent to piers or abutments.

	X/L= 0	X/L= 0.1	X/L= 0.2	X/L= 0.3	X/L= 0.4	X/L= 0.5	X/L= 0.6	X/L= 0.7	X/L= 0.8	X/L= 0.9	X/L= 1
K	586.773	436.544	382.624	351.811	297.744	314.738	729.787	832.266	926.635	1277.460	1762.350
A	158.460	633.453	700.820	723.359	463.631	364.279	0	0	141.056	-133.047	-517.389
B	0	0	0	0	0	0	-10.745	-14.041	-15.068	-18.566	-29.190
C	-15.110	-13.878	-14.589	-15.416	-11.188	-11.054	-15.802	-13.467	-13.105	-11.892	0
D	-36.718	-45.826	-41.086	-36.539	0	0	-37.169	-49.127	-68.694	-104.635	-134.375
E	0.1072	0.1288	0.1451	0.1517	0.0902	0.0945	0.0856	0.0935	0.1496	0.1921	0.1414
AB	9.507	0	0	0	12.213	11.952	9.549	5.991	0	0	13.851
AC	0	0	0	0	-9.565	-9.309	0	0	0	0	0
AD	0	-39.768	-50.028	-54.349	-63.153	-53.063	-33.919	-22.424	0	25.894	29.303
AE	0	0	0	0	0.12574	0.12149	0.14237	0.11476	0	0	0
BC	0	0	0	0	0	0	0	0	0	0	0
BD	0	1.1232	1.0972	1.1289	0	0	1.6005	2.0072	2.3764	2.8973	3.3315
BE	0	0	0	0	0	0	0	0	0	0	0
CD	0	0	0	0	0	0	0	0	0	0	0
CE	0	0	0	0	0	0	0	0	0	0	0
DE	0	0	0	0	0	0	0	0	0	0	0

K: Constant, A: Substructure configuration, B: Width, C: Span, D: Vertical clearance, E: HRRPUA

Table 13
Parametric fire curves coefficients for the web / top flange / top slab steady burning adiabatic temperatures, for fires located adjacent to piers or abutments.

	X/L= 0	X/L= 0.1	X/L= 0.2	X/L= 0.3	X/L= 0.4	X/L= 0.5	X/L= 0.6	X/L= 0.7	X/L= 0.8	X/L= 0.9	X/L= 1
K	686.808	886.323	891.939	912.422	1020.150	1129.330	1184.990	1242.040	1443.450	1462.280	1651.940
A	273.106	511.806	527.134	515.162	351.256	198.326	196.256	184.768	0	0	-283.033
B	0	-14.364	-14.456	-14.733	-19.277	-20.906	-23.090	-25.156	-29.975	-25.979	-24.989
C	-14.029	-13.950	-14.114	-14.058	-13.759	-12.773	-11.718	-10.138	-11.140	-6.148	0
D	-64.477	-95.759	-97.535	-100.176	-104.713	-119.845	-126.752	-133.754	-138.346	-162.035	-169.798
E	0.1318	0.1533	0.1668	0.1766	0.1849	0.1929	0.2023	0.2123	0.2201	0.2892	0.2569
AB	0	0	0	0	7.404	7.517	7.577	7.910	15.912	10.648	11.408
AC	0	0	0	0	0	0	0	0	0	0	0
AD	0	-26.047	-27.542	-25.613	-21.555	0	0	0	0	46.355	63.639
AE	0	0	0	0	0	0	0	0	0	-0.1467	-0.1491
BC	0	0	0	0	0	0	0	0	0	0	0
BD	0.9791	2.9134	2.8981	2.9045	2.9722	3.1397	3.4064	3.6732	3.7907	3.5933	3.3025
BE	0	0	0	0	0	0	0	0	0	0	0
CD	0	0	0	0	0	0	0	0	0	0	0
CE	0	0	0	0	0	0	0	0	0	0	0
DE	0	0	0	0	0	0	0	0	0	0	0

K: Constant, A: Substructure configuration, B: Width, C: Span, D: Vertical clearance, E: HRRPUA

Table 14
Results of MAPE values for steady burning adiabatic temperatures of existing models.

	Mean (%)	Interval (%)
Bottom flange temperatures for fire under mid-span	2.6	[1.2, 5.0]
Web/top flange/slab temperatures for fire under mid-span	1.5	[0.4, 4.0]
Bottom flange temperatures for fire adjacent to an abutment or piers	8.0	[2.8, 24.9]
Web/top flange/slab temperatures for fire adjacent to an abutment or piers	6.9	[1.3, 25.8]

Table 15
Results of PE values for maximum girder steady burning adiabatic temperatures of existing models.

PE	Mean of absolute values (%)	Interval (%)
Bottom flange temperatures for fire under mid-span	1.6%	[− 3.4, 6.0]
Web/top flange/slab temperatures for fire under mid-span	1.3%	[− 5.3, 5.8]
Bottom flange temperatures for fire adjacent to an abutment or piers	3.5%	[− 8.8, 8.4]
Web/top flange/slab temperatures for fire adjacent to an abutment or piers	3.4%	[− 7.4, 9.9]

with position X/L= 1 is a few degrees centigrade, and thus negligeable.

By comparing results from Table 14 with Table 15, it is clear that the prediction of steady burning adiabatic temperatures for the position located above the burning tanker is better than the predictions for the curve as a whole. This is due to parameters such as width or span having less influence, whilst the further we are from the fire source, the more importance these parameters acquire. These parameters are also more likely to have significant interactions with other parameters. In any case, the prediction of the maximum girder steady burning adiabatic temperatures is considered more important as they will have more influence on the global response of the bridge. Fig. 8 and Table 16 compare steady burning adiabatic temperatures obtained using the proposed parametric fire curves with those obtained from FDS models for equivalent parameter values. Predictions are excellent and generally better for the position located above the burning tanker than for the curve as a whole.

4.3. Interpolation

Table 17 details new bridge configurations with parameter values within the ranges of the configurations used to build the proposed parametric curves. These configurations are used to validate the proposed curves with models not included in their development.

Firstly, the corresponding FDS analyses for these bridge parameters have been carried out to obtain the steady burning adiabatic temperatures for each relative position. These are then compared with the steady burning adiabatic temperatures forecast by the parametric fire curves.

As can be observed graphically in Fig. 9 (for selected models) and

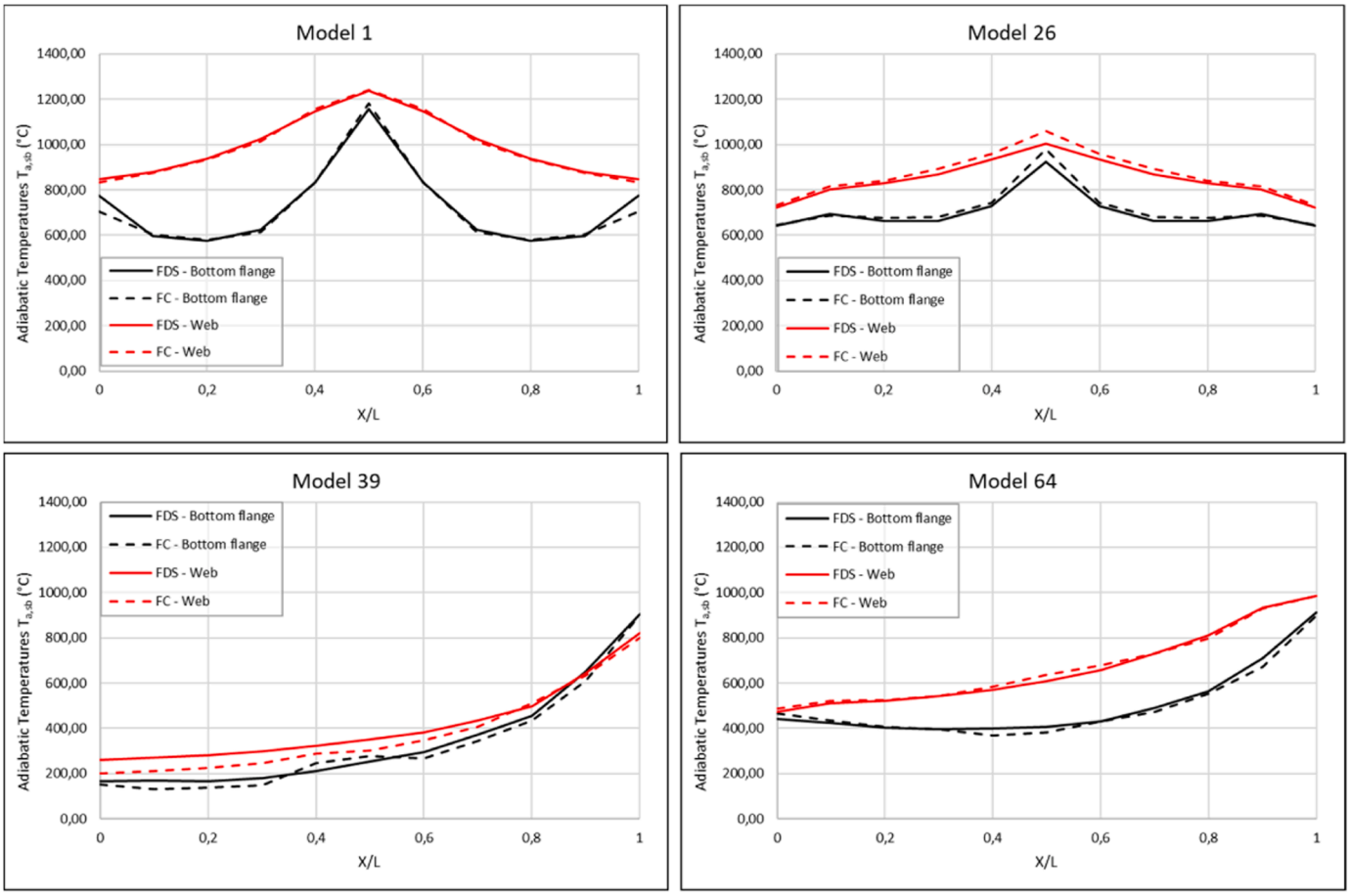

Fig. 8. Comparison of steady burning adiabatic temperatures ($T_{a,sb}$) obtained using the proposed parametric fire curves and those obtained from FDS models for equivalent parameter values, for selected existing models. Bridge configurations for each model are defined in Table 2.

Table 16
MAPE results for steady burning adiabatic temperatures (all relative positions) and PE results for maximum girder steady burning adiabatic temperatures, for both bottom flange and web / top flange / top slab for selected existing models.

MODEL	BOTTOM FLANGE		WEB / TOP FLANGE / TOP SLAB	
	MAPE	PE	MAPE	PE
Model 1	2.5%	2.0%	0.8%	0.4%
Model 26	1.9%	6.0%	2.2%	5.8%
Model 39	10.7%	-0.3%	11.8%	-2.4%
Model 64	3.2%	-1.6%	1.7%	0.1%

from the values of MAPE and PE in Table 18, the predictions of steady burning adiabatic temperatures by the parametric fire curves generally fit very well those obtained with the FDS analyses, with values of MAPE generally below 12%, with exception of model VAL-INT-7.

For this model (VAL-INT 7), the MAPE values are affected significantly by the overestimation of temperatures for the relative positions furthest from the fire location. Whilst in absolute terms the observed difference is not the largest that has been recorded when compared to the initial training data, due to the relatively low steady burning adiabatic temperatures (below 400 °C for bottom flange and 600 °C for web / top flange / lower slab) for 6 of the 11 relative positions, the percentage error is inflated.

As can be seen by the MAPE and PE values, once again the prediction of maximum steady burning adiabatic temperatures outperforms those of the curves as a whole, with the exception of model VAL-INT 3, which presents the largest values of PE for predicted maximum girder steady burning adiabatic temperatures for any of the models analyzed in this paper.

4.4. Extrapolation

Table 19 shows bridge configurations with span length values outside the ranges of those used for the existing models (training data). These configurations are used to evaluate whether the proposed

Table 17
Bridge configurations for interpolation models.

MODEL	Fire location	Substructure configuration	Width (m)	Span (m)	Vertical clearance (m)	HRRPUA (kW/m^2)
VAL-INT 1	Abutment	Open piers	13.0	20	7	2400
VAL-INT 2	Mid-span	Abutments	18.0	18	6	2400
VAL-INT 3	Mid-span	Abutments	16.0	16	6	1800
VAL-INT 4	Mid-span	Open piers	13.0	24	8	2100
VAL-INT 5	Abutment	Abutments	20.0	21	5	2100
VAL-INT 6	Mid-span	Open piers	23.4	18	7	2000
VAL-INT 7	Abutment	Abutments	13.0	23	8	2200

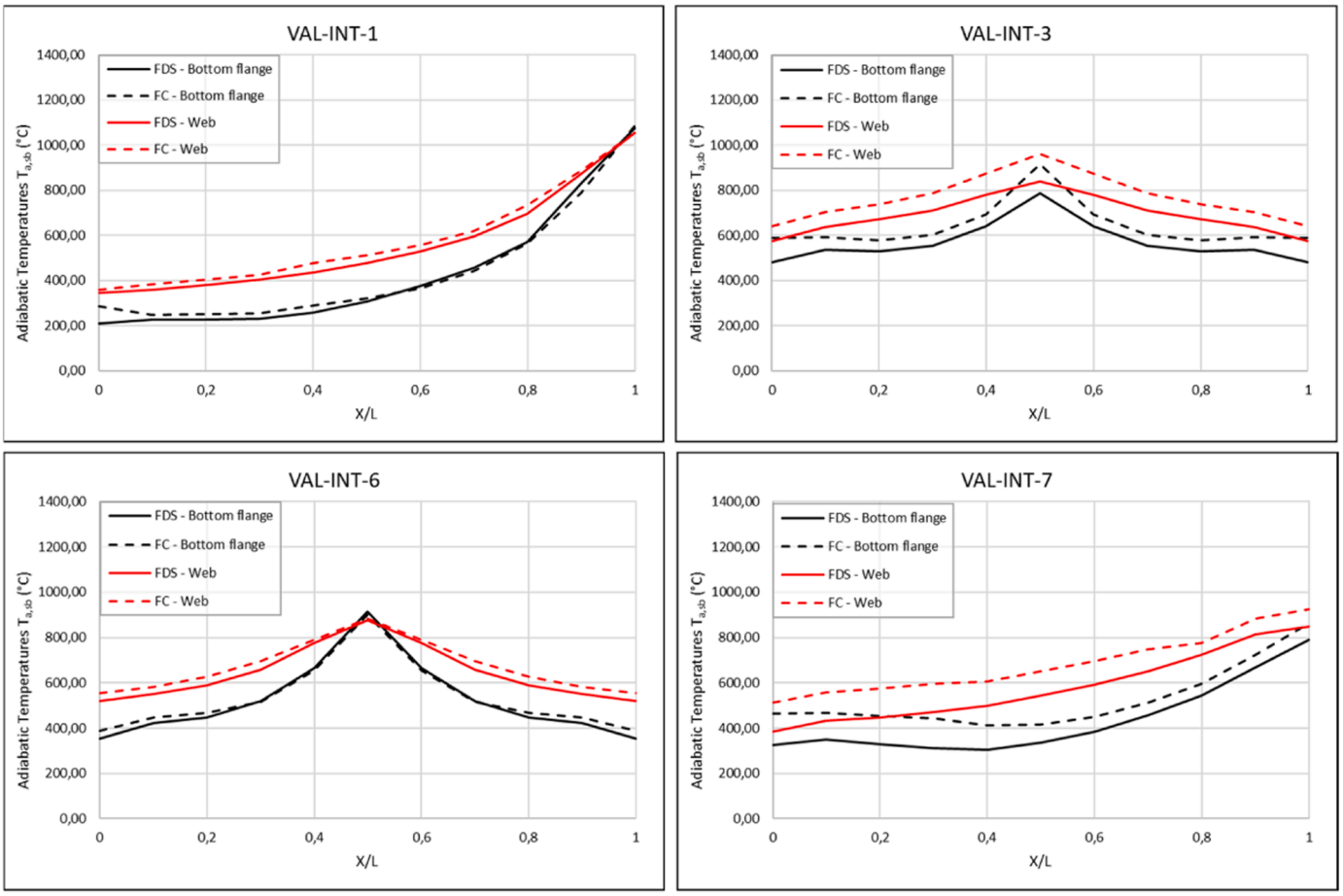

Fig. 9. Comparison of steady burning adiabatic temperatures obtained using the proposed parametric fire curves and those obtained from FDS models for equivalent parameter values, for selected interpolation models.

Table 18
MAPE results for steady burning adiabatic temperatures (considering all relative positions) and PE results for maximum steady burning adiabatic temperatures, for both bottom flange and web / top flange / top slab interpolation models.

MODEL	BOTTOM FLANGE		WEB / TOP FLANGE / TOP SLAB	
	MAPE	PE	MAPE	PE
VAL-INT 1	8.7%	1.1%	5.1%	0.0%
VAL-INT 2	10.4%	6.1%	8.6%	6.5%
VAL-INT 3	12.2%	16.7%	11.2%	14.4%
VAL-INT 4	4.0%	-0.2%	5.8%	3.4%
VAL-INT 5	7.2%	5.4%	6.6%	4.5%
VAL-INT 6	4.3%	-1.4%	4.9%	0.7%
VAL-INT 7	24.7%	9.1%	19.6%	8.8%

parametric fire curves can accurately forecast steady burning adiabatic temperatures for this new range.

Once again, the FDS analyses for these bridge parameters have been carried out, and the steady burning adiabatic temperatures for each relative position. are compared with those forecast by the parametric fire curves (see Fig. 10 and Table 20).

For the four models analyzed with spans outside the range used to obtain the parametric fire curve, the predicted steady burning adiabatic temperatures can be considered fairly accurate for all relative positions, with MAPE values below 8.2% for all models. As expected, the forecast maximum steady burning adiabatic temperatures once again outperform average of the whole curve, as span generally has less influence on the steady burning adiabatic temperatures right above or adjacent to the fire source location.

5. Conclusions

This paper presents parametric fire curves for the most fire-exposed girder of I-girder bridges heated by under-deck tanker fires. These curves incorporate a growth phase based on an ultra-fast fire curve, followed by a steady burning phase, and capture the evolving nature of fires without the need for complex CFD calculations. In addition, the curves are expressed in terms of adiabatic temperatures and, therefore, are valid for I-girder bridges with decks built with different materials (i.e. steel, concrete, composite).

The parametric curves consider two potential positions of the tanker

Table 19
Bridge configurations for extrapolation models.

MODEL	Fire location	Substructure configuration	Width (m)	Span (m)	Vertical clearance (m)	HRRPUA (kW/m^2)
VAL-EXT 1	Abutment	Abutments	13.0	13	5	2400
VAL-EXT 2	Mid-span	Abutments	13.0	13	5	2400
VAL-EXT 3	Abutment	Abutments	13.0	30	5	2400
VAL-EXT 4	Mid-span	Abutments	13.0	30	5	2400

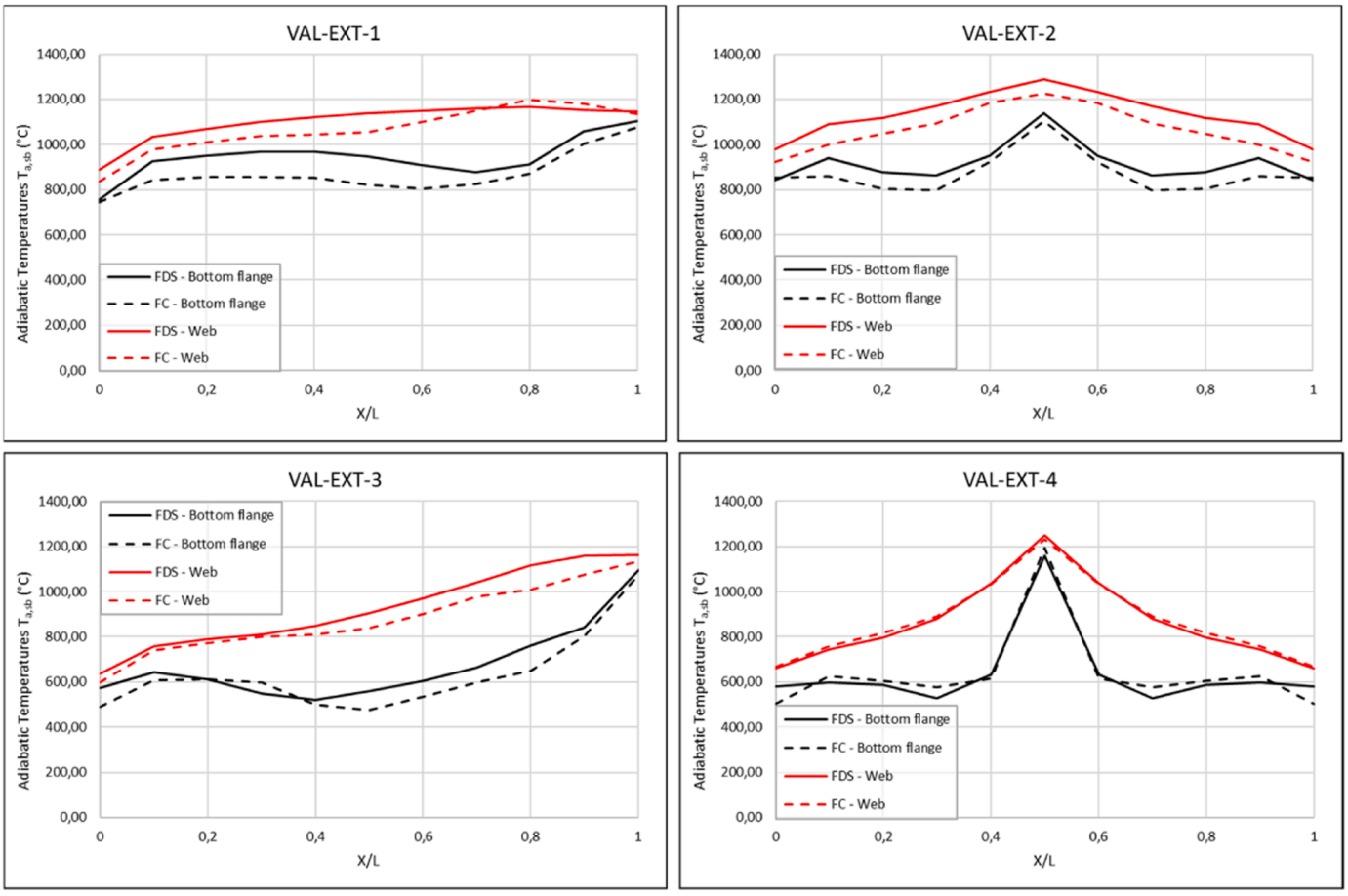

Fig. 10. Comparison of steady burning adiabatic temperatures obtained using the proposed parametric fire curves and those obtained from FDS models for equivalent parameter values, for selected extrapolation models.

Table 20
MAPE results for steady burning adiabatic temperatures (considering all relative positions) and PE results for maximum steady burning adiabatic temperatures, for both bottom flange and web / top flange / top slab extrapolation models.

MODEL	BOTTOM FLANGE		WEB / TOP FLANGE / TOP SLAB	
	MAPE	PE	MAPE	PE
VAL-EXT 1	7.8%	-2.5%	4.3%	-0.9%
VAL-EXT 2	5.5%	-3.2%	6.0%	-4.9%
VAL-EXT 3	8.2%	-1.8%	5.1%	-2.3%
VAL-EXT 4	6.2%	3.0%	1.3%	-1.4%

truck (under mid-span or adjacent to abutment/pier), and their formulation is based on five parameters: four depend on the bridge (substructure configuration, width, span and vertical clearance) and one on the type of fuel carried by the tanker (Heat Release Rate). The accuracy of the parametric fire curves is verified through validation against CFD models, affirming the robustness and reliability of the predictive models. The parametric curves are presented as straightforward mathematical expressions, facilitating their adoption by both practitioners and academics. This ease of use allows for the efficient assessment of the fire response in I-girder bridges, akin to established practices for other extreme load events. This contribution aligns with the progression of performance-based methods in bridge design, particularly in relation to fire hazards, and holds promise for strengthening bridge resilience in the face of fire incidents.

Based on the findings of the present study, future work should include the following:

- Perform further validation of the proposed parametric fire curves, to better establish the limits of their application for the studied parameters and confirm the models robustness. This could potentially lead to the proposal of suitable factors of safety that can negate any errors of the parametric fire curves when predicting steady state adiabatic temperatures.
- Study the influence of additional parameters not considered in this study, such as I-girders depth and separation, and the size, shape and position of the fire source.
- Analyze the adiabatic temperature distributions during under deck tanker fires in the transversal direction of I-girder bridges.
- Address the development of similar parametric curves for other bridge types such as box girder and slab bridges.

Supplementary material

An Excel spreadsheet is available as supplementary material to directly obtain the values of the steady burning temperatures along the I-girder bridge for the two potential tanker truck positions considered. The spreadsheet also includes the calculation of the β coefficient defined in Eq. 3, with which the growth phase of the fire curves can be calculated using Eq. 2.

CRediT authorship contribution statement

Jethro David Howard: Writing – review & editing, Writing – original draft, Visualization, Validation, Software, Methodology, Investigation, Data curation, Conceptualization. **Ignacio Paya-Zaforteza:** Writing – review & editing, Writing – original draft, Project

administration, Methodology, Investigation, Formal analysis, Conceptualization. **Guillem Peris-Sayol:** Writing – review & editing, Software, Methodology, Investigation, Formal analysis, Conceptualization..

Declaration of Competing Interest

The authors declare that they have no known competing financial interests or personal relationships that could have appeared to influence the work reported in this paper.

Data Availability

Data will be made available on request.

Acknowledgements

This work was funded by CRUE-Universitat Politècnica de València.

Appendix A. Supporting information

Supplementary data associated with this article can be found in the online version at doi:10.1016/j.engstruct.2024.117810.

References

[1] Ghosn M., Moses F., Wang J. NCHRP Report 489. Design of Highway Bridges for Extreme Events. Transportation Research Board of the National Academies 2003.
[2] Peris-Sayol G, Paya-Zaforteza I, Balasch-Parisi S, Alós-Moya J. Detailed analysis of the causes of bridge fires and their associated damage levels. J Perform Constr Facil 2017;31. https://doi.org/10.1061/(ASCE)CF.1943-5509.0000977.
[3] Garlock M, Paya-Zaforteza I, Kodur V, Gu L. Fire hazard in bridges: review, assessment and repair strategies. Eng Struct 2012;35:89–98. https://doi.org/10.1016/j.engstruct.2011.11.002.
[4] Liu Z, Li GQ, Paya-Zaforteza I, Cai CS, Huang Q. Fire hazards in bridges: state of the art, recent progress, and current research gaps. J Bridge Eng 2023;28. https://doi.org/10.1061/JBENF2.BEENG-5790.
[5] Wright W., Lattimer B., Woodworth M., Nahid M., Sotelino E. Highway bridge fire assessment draft final report. NCHRP Program Transportation Research Board of the National Academies Virginia Polytechnic Institute and State University 2013.
[6] Catalini M., Levy M. In Rubble Beneath I-95 Collapse in Philadelphia, Investigators Looking for Truck Fire's Cause. National Post 2023.
[7] Rinaudo P, Paya-Zaforteza I, Calderón PA. Improving tunnel resilience against fires: a new methodology based on temperature monitoring. Tunn Undergr Space Technol 2016;52:71–84. https://doi.org/10.1016/j.tust.2015.11.021.
[8] Hua N, Elhami Khorasani N, Tessari A. Numerical modeling of the fire behavior of reinforced concrete tunnel slabs during heating and cooling. Eng Struct 2022;258:114135. https://doi.org/10.1016/j.engstruct.2022.114135.
[9] Hua N, Elhami Khorasani N, Tessari A. Utilizing advanced modelling for fire damage assessment of reinforced concrete tunnel linings. Struct Eng Int 2023;33:586–95. https://doi.org/10.1080/10168664.2022.2161440.
[10] Zhang Y, Zhang X, Wang L. Experimental validation and simplified design of an energy-based time equivalent method applied to evaluate the fire resistance of the glulam exposed to parametric fire. Eng Struct 2022;272:115051. https://doi.org/10.1016/j.engstruct.2022.115051.
[11] Garcia-Castillo E, Paya-Zaforteza I, Hospitaler A. Analysis of the fire resistance of timber jack arch flooring systems used in historical buildings. Eng Struct 2021;243:112679. https://doi.org/10.1016/j.engstruct.2021.112679.
[12] Yan X, Gernay T. Structural fire design of load-bearing cold-formed steel assemblies from a prototype metal building. Structures 2022;41:1266–77. https://doi.org/10.1016/j.istruc.2022.05.078.
[13] Payá-Zaforteza I, Garlock MEM. A numerical investigation on the fire response of a steel girder bridge. J Constr Steel Res 2012;75:93–103. https://doi.org/10.1016/j.jcsr.2012.03.012.
[14] Alos-Moya J, Paya-Zaforteza I, Hospitaler A, Rinaudo P. Valencia bridge fire tests: experimental study of a composite bridge under fire. J Constr Steel Res 2017;138:538–54. https://doi.org/10.1016/j.jcsr.2017.08.008.
[15] Nicoletta B, Kotsovinos P, Gales J. Review of the fire risk, hazard, and thermomechanical response of bridges in fire. Can J Civ Eng 2020;47:363–81. https://doi.org/10.1139/cjce-2018-0767.
[16] Hu J, Carvel R, Usmani A. Bridge fires in the 21st century: a literature review. Fire Saf J 2021;126:103487. https://doi.org/10.1016/j.firesaf.2021.103487.
[17] Khan MA, Khan AA, Anwar GA, Usmani A. Framework for fire risk assessment of bridges. Structures 2021;33:523–32. https://doi.org/10.1016/j.istruc.2021.04.071.
[18] Alos-Moya J, Paya-Zaforteza I, Garlock MEM, Loma-Ossorio E, Schiffner D, Hospitaler A. Analysis of a bridge failure due to fire using computational fluid dynamics and finite element models. Eng Struct 2014;68:96–110. https://doi.org/10.1016/j.engstruct.2014.02.022.
[19] Timilsina S, Yazdani N, Beneberu E. Post-fire analysis and numerical modeling of a fire-damaged concrete bridge. Eng Struct 2021;244:112764. https://doi.org/10.1016/j.engstruct.2021.112764.
[20] Watson S, Nicoletta B, Kotsovinos P, Al Hamd R, Gales J. Modelling thermal performance of unloaded spiral strand and locked coil cables subject to pool fires. Struct Eng Int 2023;33:558–68. https://doi.org/10.1080/10168664.2022.2101969.
[21] Liu Z, Lou G, Hou J, Li G. Designing a two-level steel cable-stayed bridge against fires. Struct Eng Int 2023;33:569–75. https://doi.org/10.1080/10168664.2023.2171331.
[22] Gong X, Agrawal AK. Safety of cable-supported bridges during fire hazards. J Bridge Eng 2016;21. https://doi.org/10.1061/(ASCE)BE.1943-5592.0000870.
[23] Cui C, Chen A, Ma R. Stability assessment of a suspension bridge considering the tanker fire nearby steel-pylon. J Constr Steel Res 2020;172:106186. https://doi.org/10.1016/j.jcsr.2020.106186.
[24] Saglik H, Chen A, Ma R. Performance of bolted splice connection in I-girder composite bridges under tanker fire. J Constr Steel Res 2022;199:107590. https://doi.org/10.1016/j.jcsr.2022.107590.
[25] Peng X, Zhou M. Thermo-mechanical behavior of composite beams with corrugated steel webs exposed to localized fire. J Constr Steel Res 2023;211:108180. https://doi.org/10.1016/j.jcsr.2023.108180.
[26] Yan X, Gernay T. Numerical modeling of localized fire exposures on structures using FDS-FEM and simple models. Eng Struct 2021;246:112997. https://doi.org/10.1016/j.engstruct.2021.112997.
[27] Pagán-Martínez JJ, Paya-Zaforteza I, Hospitaler-Pérez A. Post-fire assessment of composite steel-concrete box-girder bridges: lessons from a recent incident. J Constr Steel Res 2024;214:108425. https://doi.org/10.1016/j.jcsr.2023.108425.
[28] Beneberu E, Yazdani N. Performance of CFRP-strengthened concrete bridge girders under combined live load and hydrocarbon fire. J Bridge Eng 2018;23. https://doi.org/10.1061/(ASCE)BE.1943-5592.0001244.
[29] Wu X, Huang T, Au FTK, Li J. Posttensioned concrete bridge beams exposed to hydrocarbon fire. J Struct Eng 2020;146. https://doi.org/10.1061/(ASCE)ST.1943-541X.0002791.
[30] Selamet S, Ozer AY, Ildan KB. Experimental study on the fire performance of prestressed steel parallel wire strands. Eng Struct 2023;280:115709. https://doi.org/10.1016/j.engstruct.2023.115709.
[31] Jeanneret C, Nicoletta B, Robertson L, Gales J, Kotsovinos P. Guidance for the post-fire structural assessment of prestressing steel. Eng Struct 2021;235:112023. https://doi.org/10.1016/j.engstruct.2021.112023.
[32] Kragh E, Narasimhan H, Jensen JL. Fire protection of bridge cables. Struct Eng Int 2020;30:530–3. https://doi.org/10.1080/10168664.2020.1716653.
[33] Eurocode 1: Actions on structures - Part 1–2: General actions - Actions on structures exposed to fire. COMITE EUROPEEN DE NORMALISATION (CEN); 2002.
[34] Choi J. Concurrent fire dynamics models and thermomechanical analysis of steel and concrete structures. Ph.D. Thesis. Georgia Institute of Technology, USA, 2008.
[35] Ma R, Cui C, Ma M, Chen A. Numerical simulation and simplified model of vehicle-induced bridge deck fire in the full-open environment considering wind effect. Struct Infrastruct Eng 2021;17:1698–709. https://doi.org/10.1080/15732479.2020.1832535.
[36] Wu X, Huang T, Au FTK, Li J. A localized fire model for predicting the surface temperature of box girder bridges subjected to tanker truck fire. Fire Technol 2020;56:2059–87. https://doi.org/10.1007/s10694-020-00966-2.
[37] Lattimer BY. Heat fluxes from fires to surfaces. SFPE Handbook of Fire Protection Engineering. 5th ed. Greenbelt, MD, USA: National Fire Protection Association; 2016. p. 745–98.
[38] Farhey D. Structural performances of bridge types in the U.S. National Bridge Inventory. Infrastruct (Basel) 2018;3:6. https://doi.org/10.3390/infrastructures3010006.
[39] Peris-Sayol G, Paya-Zaforteza I, Alos-Moya J, Hospitaler A. Analysis of the influence of geometric, modeling and environmental parameters on the fire response of steel bridges subjected to realistic fire scenarios. Comput Struct 2015;158:333–45. https://doi.org/10.1016/j.compstruc.2015.06.003.
[40] Faber TE. Fluid dynamics for physicists. Cambridge University Press; 1995. https://doi.org/10.1017/CBO9780511806735.
[41] Mayfield C, Hopkin D. Design fires for use in fire safety engineering. IHS BRE Press; 2011.
[42] Buchanan AH, Abu AK. Structural design for fire safety. Wiley; 2016. https://doi.org/10.1002/9781118700402.
[43] Wickström U., Duthinh D., McGrattan K. Adiabatic Surface Temperature for Calculating Heat Transfer to Fire Exposed Structures. 11th International Interflam Conference, London, England: 2007, p. 943–953.
[44] Alos-Moya J, Paya-Zaforteza I, Hospitaler A, Loma-Ossorio E. Valencia bridge fire tests: validation of simplified and advanced numerical approaches to model bridge fire scenarios. Adv Eng Softw 2019;128:55–68. https://doi.org/10.1016/j.advengsoft.2018.11.003.
[45] Babrauskas V. Heat release rates. SFPE handbook of fire protection engineering. 5th ed..,. Greenbelt, MD, USA: National Fire Protection Association; 2016.
[46] China Shandong Panda Mechanical Co. Ltd. Fuel Tank Truck Trailer Specification & Dimension & Weight n.d. https://www.pandamech.com/product/fuel-tank-truck-trailer-specification (accessed February 7, 2024).
[47] Bajwa CS, Easton EP, Adkins H, Cuta J, Klymyshyn N, Suffield S. The MacArthur maze fire and roadway collapse: a "Worst Case Scenario" for spent nuclear fuel transportation? Volume 7: operations, applications and components. American Society of Mechanical Engineers; 2012. p. 261–9. https://doi.org/10.1115/PVP2012-78637.

[48] McGrattan K., McDermott R., Weinschenk C., Overholt K., Hostikka S., Floyd J. Fire Dynamics Simulator Technical Reference Guide Volume 1: Mathematical Model. Gaithersburg, MD: 2013. https://doi.org/10.6028/NIST.SP.1018.
[49] US Department of Transportation FHA. Standard Plans for Highway Bridges. Volume II. 1982.
[50] Howard J.D. A proposal of design fire curves for I-girder bridges. Application to an overpass on U.S. Route 1 in Trenton, New Jersey, USA. Master's Thesis. Universitat Politècnica de València, Spain, 2019. http://hdl.handle.net/10251/128856 (accessed February 7, 2024).
[51] Kutner M, Nachtsheim C, Neter J, Li W. Applied Linear Statistical Models. 5th ed. Irwin, New York: McGraw-Hill; 2005.
[52] Taguchi G, Chowdhury S, Wu Y. Taguchi's quality engineering handbook. Wiley; 2004. https://doi.org/10.1002/9780470258354.
[53] McGrattan K. Verification and Validation of Selected Fire Models for Nuclear Power Plant Applications. Volume 7: Fire Dynamics Simulator (FDS). 2007.
[54] Hurley MJ. SFPE Handbook of Fire Protection Engineering. 5th ed. Greenbelt, MD, USA: National Fire Protection Association; 2016. https://doi.org/10.1007/978-1-4939-2565-0.
[55] StatPoint Technologies Inc. STATGRAPHICS® Centurion XVI User Manual 2009.